ORNL/TM-2022/2568

Pressurized Tube Creep Testing of Graded Transition Joints (GTJ) for G91 and 347H Base Metals

Hong Wang
Jeremy Moser
Edgar Lara-Curzio
Peeyush Nandwana

August 2022

OAK RIDGE National Laboratory

ORNL IS MANAGED BY UT-BATTELLE LLC FOR THE US DEPARTMENT OF ENERGY

ORNL/TM-2022/2568

Materials Science and Technology Division

PRESSURIZED TUBE CREEP TESTING OF GRADED TRANSITION JOINTS (GTJ) FOR G91 AND 347H BASE METALS

Hong Wang, Jeremy Moser, Edgar Lara-Curzio, Peeyush Nandwana

August 2022

Prepared by
OAK RIDGE NATIONAL LABORATORY
Oak Ridge, TN 37831
managed by
UT-BATTELLE LLC
for the
US DEPARTMENT OF ENERGY
under contract DE-AC05-00OR22725

CONTENTS

LIST OF FIGURES

LIST OF TABLES

ABSTRACT

This report briefly describes part of the research activities dedicated to a DOE FE project, graded transition joints (GTJ) development for G91 and 347H steels. The task was focused on pressurized tube creep testing on the 3D-printed GTJ materials.

A specimen with reduced gage section is developed that includes G91, GTJ, and 347H subsections. A tapered GTJ subsection is introduced to address the technical challenge of mechanical testing with mismatched rupture times of the base metals. The report provides the descriptions of basic considerations, specimen preparation, testing system, and experimental results along with main findings.

1. INTRODUCTION

Current mechanical testing of graded transition joints (GTJ) for dissimilar metal welds (DMW) is conducted by following ASME Boiler and Pressure Vessel Code, Section IX: Welding and Brazing.

The testing and evaluation of DMW can be dated back to those for G91 and 304 SS, for example, by Sikka et al.[1] Usually, a specimen of sheet,[2,3,4] square,[5] or round shape[6,7,8] is made of a cross weld for tensile or creep tests. Such practice has been exercised for the study of DMWs in a wide variety of base metals.

The main issue of these test methods is associated with the uniform cross section area that extends over dissimilar base metals and weld. In the work where the study focuses on the deformation of materials, the loading can be controlled within the safety regions of both base metals. For the study that targets both large deformation and failure, the loading would result in a premature failure if the strength or rupture time of one base metal is weaker or shorter than the other, and that is usually the case.

In applications of pipe or tube, a transition piece is used to join the dissimilar metals, where the wall thickness of the transition varies gradually from one end to the other and forms a tapered shape. So, the life of components can be maximized. The concept and related issues were discussed on several occasions previously.[9,10,11,12] In addition, tube material under the pressurization is subjected to a loading of multi-axial stress state. Testing of the material under such condition can provide the insight of failure mechanisms closer to the applications than a uniaxial stress loading. However, the experimental approach has not been implemented for the GTJ in a laboratory setting, and no data are available.

This report describes part of the research activities and experimental results dedicated to GTJ development for G91 and 347H steels. The study was focused on pressurized tube creep testing on the printed GTJ materials. The following sections provide some background and descriptions of our specimen design, testing system, and experimental results along with some discussions.

2. BACKGROUND AND CONSIDERATIONS

2.1 TUBE STRESS AND YIELD CRITERION

For a tube with an internal pressure p, internal radius R_i, and external radius R_o, the tangential or hoop stress (σ_t), axial stress (σ_a), and radial stress (σ_r) at radial location (r) can be calculated per the following equations[13]

$$\sigma_t = p\frac{R_i^2}{R_o^2 - R_i^2}\left(1 + \frac{R_o^2}{r^2}\right),$$
$$\sigma_a = p\frac{R_i^2}{R_o^2 - R_i^2},$$
$$\sigma_r = p\frac{R_i^2}{R_o^2 - R_i^2}\left(1 - \frac{R_o^2}{r^2}\right).$$

Equation 1

For a thin-walled tube whose ratio of wall thickness to diameter of tube is around or less than 0.1, there are

$$\sigma_t = \frac{pR_i}{h},$$
$$\sigma_a = \frac{pR_i}{2h},$$
$$\sigma_r = 0,$$

Equation 2

where h is the wall thickness of tube. For multiaxial stress state, an effective or equivalent stress needs to be defined and evaluated according to specified yield criterion.

1) Von Mises stress σ_{VM} considers all three principal stresses (hoop, axial and radial in tube wall):

$$\sigma_{VM} = \frac{1}{\sqrt{2}}\left[(\sigma_1 - \sigma_2)^2 + (\sigma_2 - \sigma_3)^2 + (\sigma_3 - \sigma_1)^2\right]^{1/2}$$

Equation 3

2) Stress intensity (SI) σ_{SI} is two times the Tresca stress or the maximum principal stress minus minimum principal stress:

$$\sigma_{SI} = \sigma_{\max} - \sigma_{\min}$$

Equation 4

As can be seen, these effective stresses depend on the radial position (r); usually, the stress at the inner surface is higher than that at the outer surface. For thin-wall tube, the effective stress can be simplified. For example, the Mises stress can be reduced to

$$\sigma_{VM} = \frac{\sqrt{3}}{2}\frac{pR_i}{h}$$

Equation 5

3) An alternative is reference stress σ_{ref} that is based on a limited load analysis of perfectly plastic material:

$$\sigma_{ref} = \frac{p}{\ln(R_o / R_i)}.$$

Equation 6

The limited load is defined when the entire tube thickness reaches yield, and therefore, the effective stress depends only on the size of tube, but not the position. The derivative of above equation also makes use of stress intensity (maximum shear stress) criterion.

Both Mises stress and stress intensity are used to describe the yielding condition of ductile materials. This study will begin with Mises stress criterion as it has been shown to be widely acceptable for the structural steels.

These stress equations can be used to estimate the stress once pressure and tube geometric size are determined. It can also be used to calculate the pressure if the target stress and tube size are provided.

2.2 LARSON-MILLER (LM) ANALYSIS OF G91 AND 347H

For high temperature applications, the mechanical strength of material is generally time- dependent. To account for the time dependence, Larson Miller analysis was used in this study to determine the strength of material at given creep time and temperature conditions, including G91 and 347H.

The G91 creep data were based on a report by Swindeman et al. (2007).[14] A polynomial of log(S) of degree three were used, in which S is rupture stress. The coefficients of polynomial were obtained by curve-fitting and the stresses estimated for various temperatures and rupture times. Stress vs. rupture time curves at various temperatures are shown in Figure 1 along with those of 347H. The data for 347H were taken from the reference.[15] In the time-dependent region, the strength of 347H is usually higher than G91 for a given rupture time and temperature.

A creep test with high temperature and short rupture time was pursued in this study; namely, 650 degree C and 500 h rupture time. To achieve such goal, a creep stress 165MPa (24 ksi) would be required for 347H; for G91, the required stress will be 103 MPa (14.9 ksi).

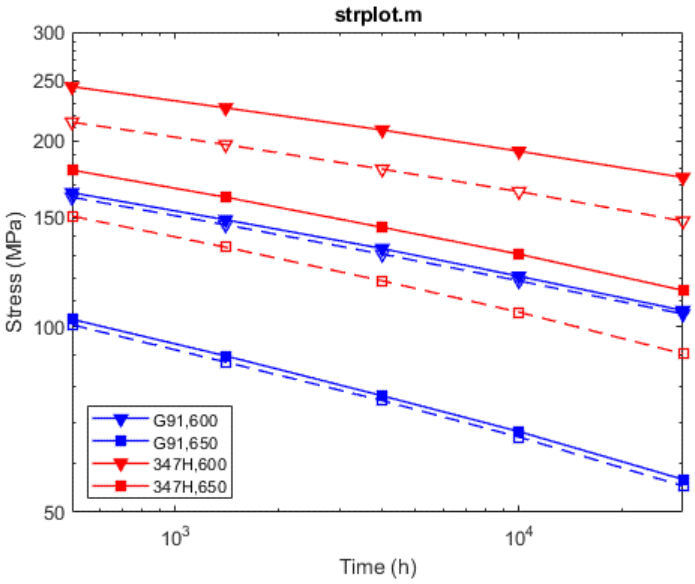

Figure 1 Creep stress as a function of time at various temperatures (degree C) for G91 and 347H, based on Larson-Miller analysis; dash lines are the lower bounds of 90% confidence level of estimate.

2.3 DESIGN CONCEPT FOR MISMATCHED RUPTURE TIMES

To evaluate the rupture behavior of GTJ effectively, the base metals are expected to have equal rupture time, or a premature failure would occur. In pressurized tube creep test, the wall thickness of G91 section needs to be larger than 347H section to compensate the lower strength at the target temperature.

In the case of graded transit joint, the mechanical strength is expected to vary gradually while the composition changes. As a result, gradual change of wall thickness is proposed to accommodate the composition gradient. This is shown in the diagram below where GTJ has a tapered section for a smooth transit (Figure 2).

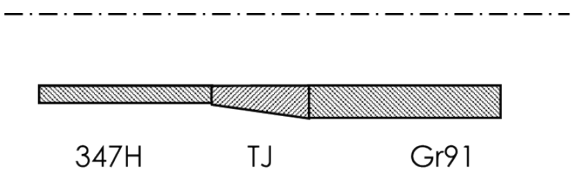

Figure 2 Specimen design concept with tapered section for GTJ

2.4 DIMENSIONS OF SPECIMEN AND TESTING PRESSURE

A specimen with reduced gage section was used whose design of tube specimen followed general guideline as follows,

- Tube outside diameter (OD) is selected to make full use of materials available
- Tube thickness is about 10% of OD to meet thin tube requirement but needs to include enough number of grains like 10 grains
- Gage length is about 6 - 10 times the tube OD to control the constraining effect of end caps
- The tube OD and wall thickness are subjected to the capacity of pressure system and estimate rupture time

For 650 degree C and 500 h rupture time as discussed, the creep stress would be 165MPa (24 ksi) for 347H and 103 MPa (14.9 ksi) for G91. These creep stresses are the equivalent stresses, or σ_{eq}, for the respective tube subsections. The above considerations resulted in the following design of specimen components.

- 347H section of tube specimen: OD 14.33 mm (0.564 in.), wall thickness 1.40 mm (0.055 in), inside diameter (ID) 11.52 mm (0.454 in.), length 71.58 mm (2.818 in.).
    - End cap: OD is 17.12 mm (0.674 in.), ID 11.52 mm (0.454 in), and overall length is 25.40 mm (1 in.).
    - The end cap features a step hole: one end has a diameter of 0.256 in. to accommodate a ¼ in. diameter high-pressure tube, and opposite end a diameter of 0.084 in. as a conduit of gas.
- G91 section of tube specimen: OD 16.0 mm (0.630 in), wall thickness 2.24 mm (0.088 in), ID 11.52 mm, and length 80.01 mm (3.15 in).
    - End cap OD is 20.47 mm (0.806 in.), ID 11.52 mm, and overall length is 25.4 mm (1 in).
- GTJ section: OD varying from 14.33 mm (0.564 in.) on 347H side to 16.0 mm (0.630 in.) on G91 side, ID 11.52 mm (same as those of 347 and G91 sections), and a length of 11.99 mm (0.472 in).
    - The average stress of GTJ is 134 MPa, and stress gradient 5.17 MP/mm.

The overall length of tube assembly is 214.38 mm (8.44 in). A high-pressure 316 SS tube is inserted in 347H end cap. All the parts were assembled by using welding to be discussed.

The inner pressure was estimated to be 46.26 MPa (6,710 psi) according to Equation 5.

The plots in Figure 3 illustrate how the OD varies from 347H end to G91 end along with those of stress condition and rupture time.

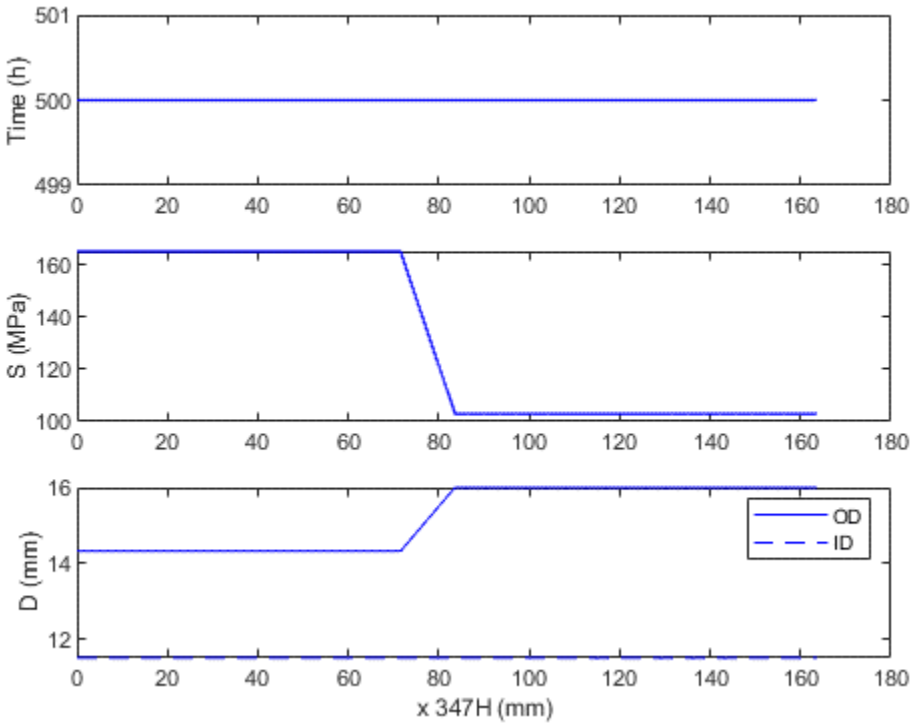

Figure 3 Implementation of the design concept of tube specimen with a tapered section GTJ section where OD and stress change in transition: 1) rupture time in upper view, 2) stress in middle view, and 3) inner and external diameters in lower view; x is measured from the 347H end of gage section

3. SPECIMEN PREPARATION

3.1 MATERIALS

GTJ materials were manufactured by using 3D- printing in Deposition Group, MS&TD, ORNL. Two specimens were prepared one for each material, Table 1.

Table 1 GTJ Materials for testing

No	Specimen	GTJ Material
1	GTJ 50/50	Composition of G91 varying from G91 side to 347H side in a ratio of 50/50, and the material had a size of 12× 30.3× 16.90 mm with 12 mm direction as deposition direction
2	GTJ 100/80/60	Composition of G91 varying from G91 side to 347H side in a ratio of 100/80/60/50/40/20/0: 12× 30.3× 16.90 mm with 12 mm direction as deposition direction

For base metals, tubular materials like A213 T91/ TP347H for the specified dimensions were not available. It was thus determined to machine the tube from plate material. The following plate materials were purchased for this purpose:

- A grade 91 class2 plate, 1”x12”x12”, SA387, supplied by Wingate Alloys, Inc. (Cleveland, OH)
- A 347H plate, 1”x12”x12”, SA240, supplied by Penn Stainless Products (Quakertown, PA)

The base metal section of tube specimens was machined along the rolling direction of plates.

3.2 SPECIMEN ASSEMBLY

- Gas tungsten arc welding (GTAW) was used to assemble the subsections of specimen and the feed gas tube.
- G91 and 347 wires were used as filler materials. For the welds with G91, post-weld heat treatment (PWHT) to 750 deg. C, 45 min was used per ASME B31.1. An assembled specimen is shown in Figure 4.

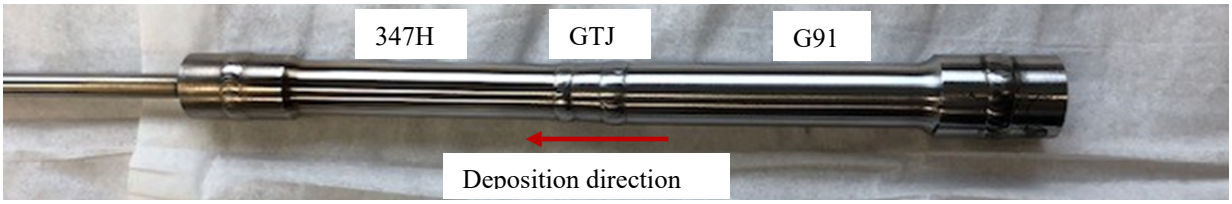

Figure 4 Assembled tube specimen whose subsections from left to right are: 347H, GTJ (deposition is pointed to the left), G91

4. TESTING SYSTEM AND TESTING PROCEDURE

4.1 HIGH-PRESSURE CAPSULE TESTING SYSTEM

The ORNL high-pressure capsule testing facility consists of: (1) a pressure booster pump (PBP), (2) a high-pressure manifold (HPM) system to supply pressure, (3) test stations (TS) for capsules with cover gas and leak detection, (4) furnaces, (5) evacuation pumping systems for the canister and capsule, and (6) a data acquisition system. The setup of GTJ specimen on the test stage is shown in Figure 5 where a steel canister (not shown) was installed around the specimen to protect the furnace.

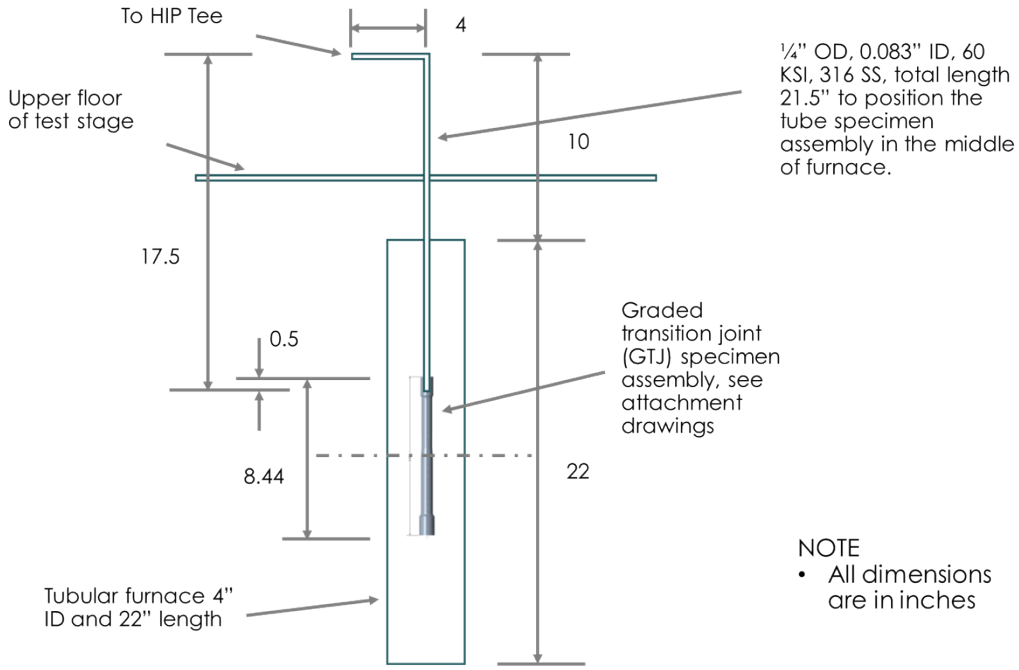

Figure 5 Diagram showing the specimen setup

4.2 PERIODICALLY INTERRUPTED CREEP TEST

To track the creep deformation of tube, testing was interrupted periodically. The procedure involves the following steps:

1) Measure and record the initial specimen diameters and specimen overall/ tangent lengths at room temperature using caliper or Keyence system. The Keyence is a non-contact method and was used for the tapered section measurement like GTJ subsection
2) Install the tube assembly in the furnace. Start data acquisition.
3) Heat and pressurize the specimen to a target temperature and pressure, and subject the specimen to the temperature and pressure conditions for a designed testing time.
4) When the time reaches, de-pressurize and cool the specimen in the furnace, and take the specimen off the ST.
5) Measure and record the specimen diameters and specimen lengths at room temperature, and if no rupture occurs, go to step 2).

Such test procedure was also used in other relevant pressurized tube creep tests.[16,17,18,19]

4.3 CHARACTERIZATION OF GTJ SPECIMEN DEFORMATION

We conducted the diametrical and axial measurements in all the subsections of tube specimen.

1) The measurement times: pre-test, 1 h, 24 h, 168 h, 400 h, and after rupture
2) The measurement quantities: diameters at nine axial positions, and axial lengths at five sections; each size is measured three times in three orientations as shown in Figure 6. Note that the D number increases from 347H end.

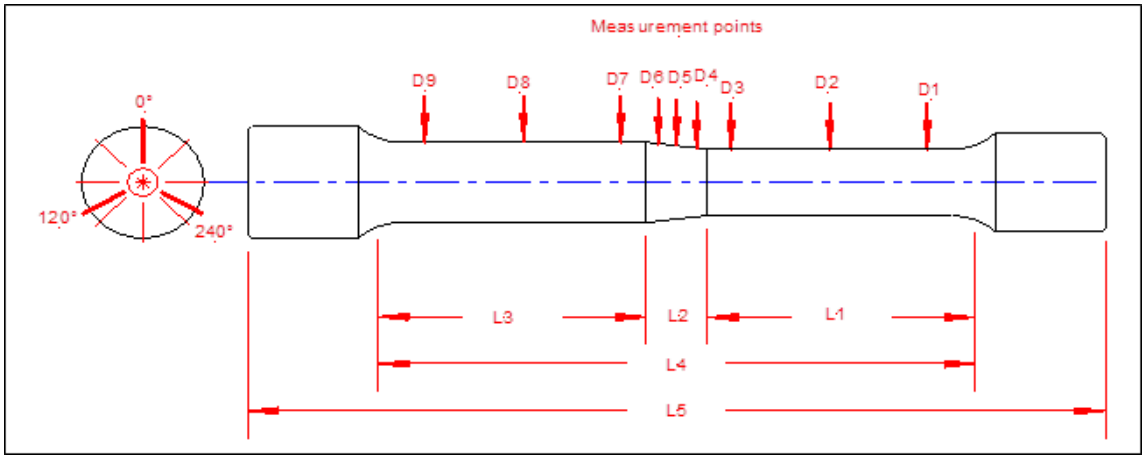

Figure 6 Quantities used for characterizing the creep deformation of GTJ tube specimen

4.4 DATA PROCESSING

The tangential strain, ε_t, was obtained according to the expression as follows

$$\varepsilon_t = \frac{\Delta D}{D_0}$$

Equation 7

where ΔD and D_0 are the diametric change and initial diameter of tube. Tangential strain rate, $\dot{\varepsilon}_t$, was obtained by using incremental strains at the time intervals as follows

$$\dot{\varepsilon}_t = \frac{\Delta \varepsilon_t}{\Delta t}$$

Equation 8

The axial strain, ε_a, was obtained according to the expression as follows

$$\varepsilon_a = \frac{\Delta L}{L_0}$$

Equation 9

where ΔL and L_0 are the length change and initial length of tube subsections. The axial strain rate can be estimated accordingly,

$$\dot{\varepsilon}_a = \frac{\Delta \varepsilon_a}{\Delta t}$$

Equation 10

The strain in radial or wall thickness direction was not measured directly in this study. Based on the volume constancy, the radial strain rate, $\dot{\varepsilon}_r$, can be estimated as follows

$$\dot{\varepsilon}_r = -\dot{\varepsilon}_t - \dot{\varepsilon}_a$$

Equation 11

5. EXPERIMENTAL RESULTS

5.1 GTJ 50/50

5.1.1 Rupture Time

The specimen failed within the G91 section with a sizable longitudinal opening. The GTJ and the welds sustained the high-temperature pressurized creep loading. The specimen had a rupture time of 22.3 h, which is much shorter than the expected.

The discrepancy between the target life and observed life deserves some comments. First, for a rupture time of 22.3 h, the LM curve of G91 at 650 degree C suggests that a creep stress of 147.6 MPa would be experienced. This stress level is obviously higher than what was suggested for G91 section, 103 MPa. Second, let's take a brief look at several factors that may have impact on the design of tube specimen.

- Use of the thin-wall tube equation may underestimate the stress level, considering h/OD = 0.14 in the G91 section and the high inner pressure.
    a. For a pressure of 46.26 MPa, the Mises stress varies from 166.37 at the inner surface to 86.24 MPa at the external surface. Use of the local Mises stress could lead to overestimate or underestimate of overall tube stress, depending on the application. For creep test tube design, averaged stress can be used; the averaged Mises stress was estimated as 119.79 MPa.
- The G91 tube material may follow a yield criterion other than Mises condition.
    a. For the pressure applied, stress intensity would vary from 192.11 MPa at the inner surface to 99.59 MPa at the outer surface, corresponding to an averaged stress intensity of 138.32 MPa;
    b. Reference stress is estimated as 140.82 MPa.

If using the averaged in evaluation, these criteria produced different stresses for the given inner pressure as can be seen. For a rupture time of 22.3 h at 650 degree C, the suggested creep stress (147.6 MPa) indicates that the thin-wall tube equation underestimated the tube stress and, at the same time, the failure of G19 section more followed the reference stress criterion.

5.1.2 Creep Deformation

5.1.2.1 Tangential strain

The tangential strain profiles are illustrated in Figure 7 where x is measured from the end face of 347H endcap. Before the failure, the strain was higher in 347H than G91. In the GTJ, the middle point (D5) had a strain equal to that of 347H. Near the welds between GTJ and the respective base metals 347H and G91, the tangential strain was lower than surrounding areas, which might be associated with the constraining effect of welds. The strain within G91 section increased significantly as expected upon the failure.

The results as a function of time are shown in Figure 8. Note that the measured strain is total strain, including loading & creep strains. The following are main observations.

- The ultimately high level of creep took place in the G91 section. The largest deformation was 16% at D7 around the fracture.
- Except the point over opening, majority of the gage sections were within 0.5 to 3.5 %.

- An intermediate creep zone existed in the GJT section. At D5, the maximum creep was around 1.8%.

For the strain rate, it can be seen:

- The strain rate was high at first hour. It attained a range of 0.4 to 1.0 %/h. As notified above, the deformation at 1 h, in fact, contains the plastic deformation from loading strain. So does the strain rate.
- The subsequent strain rate, for example, at 22.3 h, measures the creep rate. The rate was lowered in most of the part of specimen, except D7. In the latter, the rate increased from 0.556 to 0.714 %/h.
- Within the GTJ section, the rate ranged between 0.0144 and 0.0367 %/h at the specimen failure (22.3 h).

The main tangential creep rate results are summarized in Table 2 for the final creep stage.

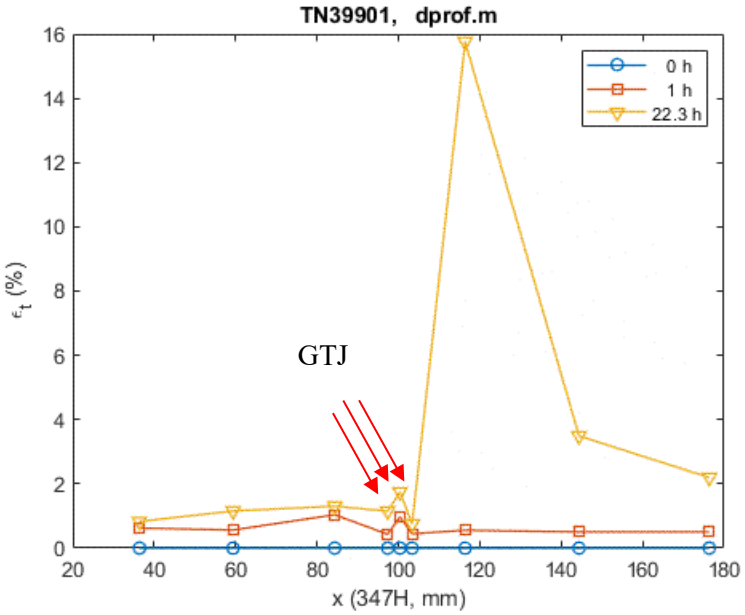

Figure 7 Profiles of tangential strain for GTJ 50/50 at various creep times where x is measured from 347H end; 650°C, inner pressure 46.26 MPa (6,710 psi). Three diameter measurement points in GTJ section are indicated by arrows.

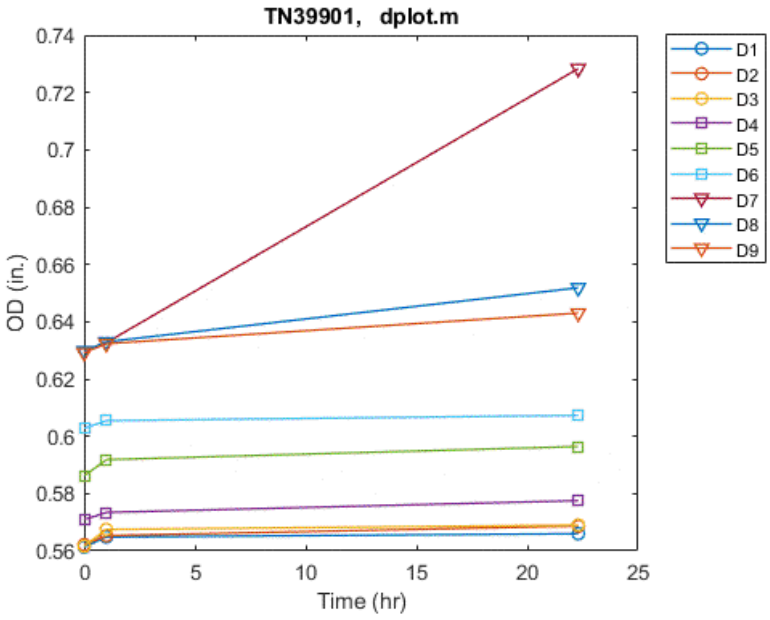
TN39901, dplot.m
OD (in.)
Time (hr)
D1
D2
D3
D4
D5
D6
D7
D8
D9

(a)

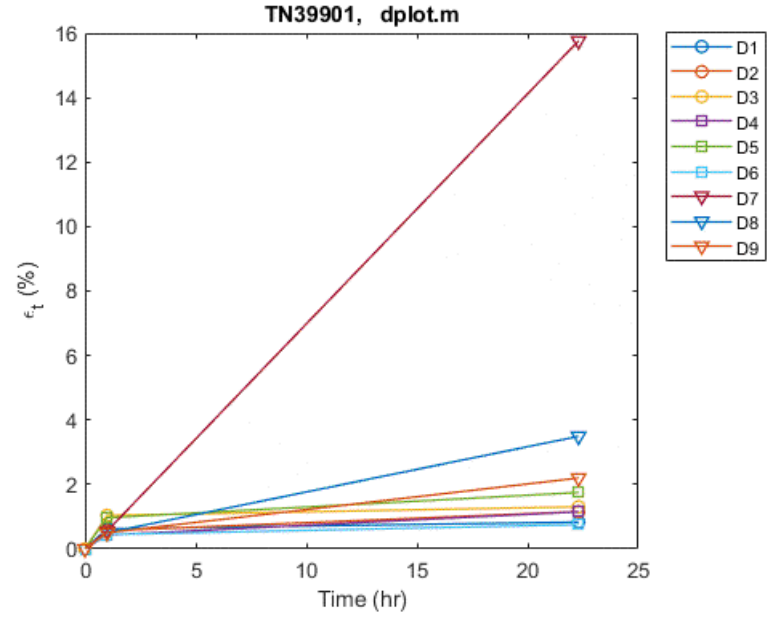
TN39901, dplot.m
ϵ_t (%)
Time (hr)
D1
D2
D3
D4
D5
D6
D7
D8
D9

(b)

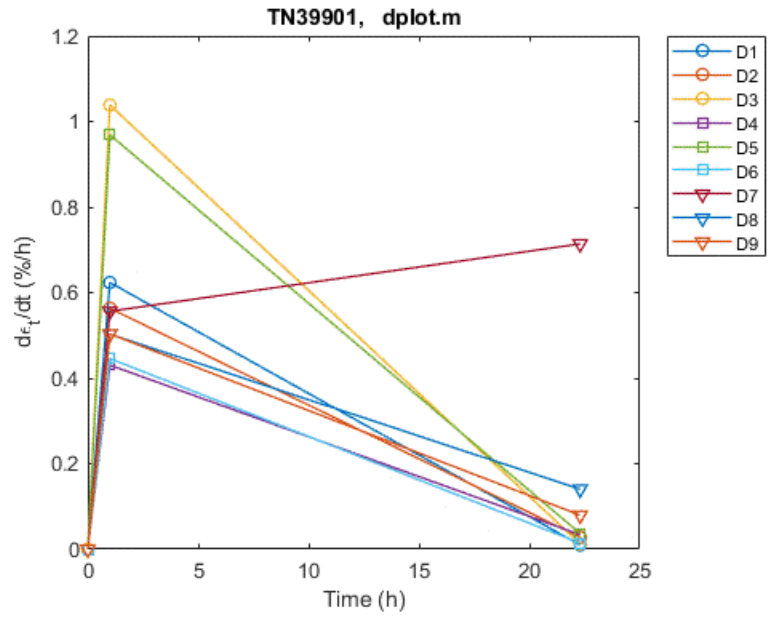

(c)

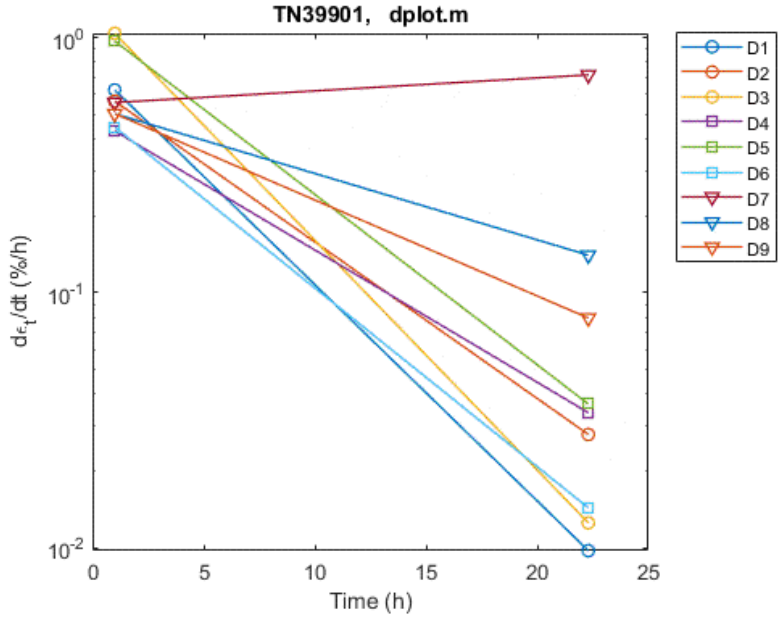

(d)

Figure 8 Variations of (a) diametric deformation, (b) tangential strain, (c) strain rate, (d) same as (c) with log scale in y-axis for GTJ 50/50; 650°C, inner pressure 46.26 MPa (6,710 psi)

Table 2 Tangential creep rates of various subsections

Spec.	Subsect.	Equiv. Stress	Stress Gradient	Creep Time	Avg. Tang. Rate	Max. Tang. Rate
		MPa	MPa/mm	h	%/h	%/h
GTJ 50/50	347H	165		22.3	1.67E-02	2.78E-02
	GTJ	134	5.17	22.3	2.83E-02	3.67E-02
	G91	103		22.3	3.11E-01	7.14E-01

GTJ 100/80/60	347H	165		38	2.27E-02	2.40E-02
	GTJ	134	5.17	38	1.25E-02	2.08E-02
	G91	103		38	1.67E-01	2.38E-01

5.1.2.2 Axial strain

The results for axial deformation, strain, and strain rate are shown in Figure 9 as a function of time.

- In the axial direction, there were a contraction of less than 15% in G91 section L3, 2% in GTJ section L2 and
- an expansion of more than 15% in 347H section L1.

Most of the axial deformations related to L1 and L3 occurred at 1 h. As discussed above, the amount of the measurement at 1 h was contributed by both loading and creep. If focusing on 347H section as measured by L1, the strain rate at 1 h was several orders of magnitude higher than that at 22.3 h, indicating substantial contribution by loading strain. On the other hand, the G91 section contracted almost same amount of expansion experienced by 347H section; however, it expanded later as validated by the positive creep rate. Note that the creep rate data in (d) are same as those in (c) but shown with log scale so that the negative points are not displayed.

The axial creep rate results are summarized in Table 3 for the final creep stage. It is interesting to see that the GTJ section showed a higher axial rate than other two sections. The strain rate in axial direction was more or less than those in tangential direction, depending on subsection. For example, the axial rate in the GTJ section exceeded the averaged tangential strain rate (ratio of 1.03). The axial strain rate in the G91 section, even after it turned into expansion, was much lower than that of tangential strain rate, which is expected because of large bulging around the opening, with a ratio of 0.04.

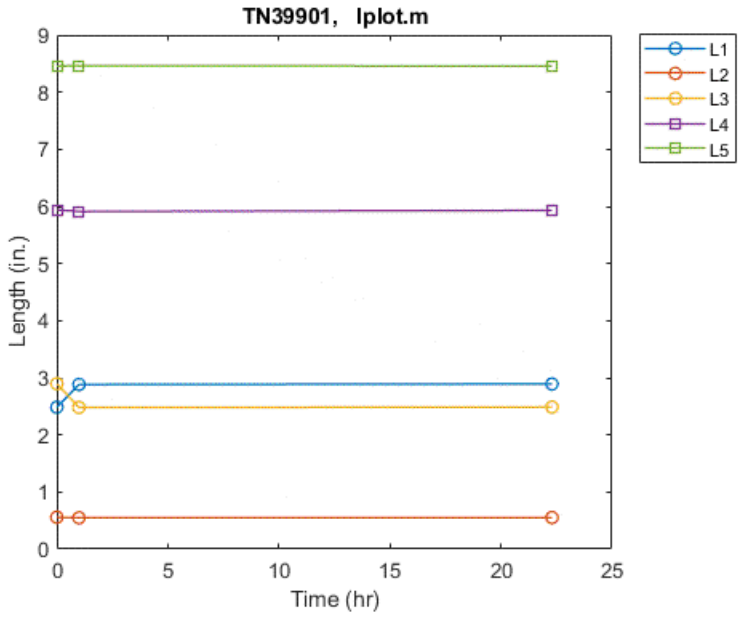

(a)

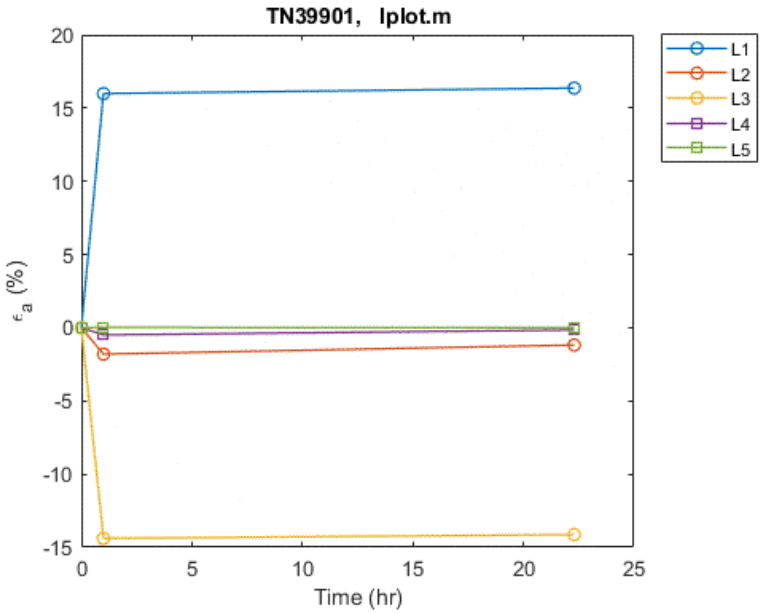
TN39901, lplot.m
L1
L2
L3
L4
L5
ϵ_a (%)
Time (hr)

(b)

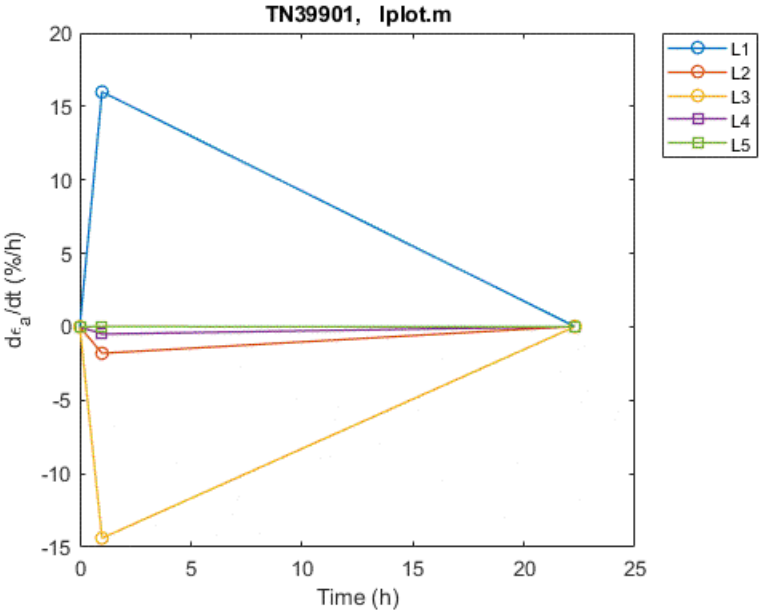
TN39901, lplot.m
L1
L2
L3
L4
L5
$d\epsilon_a/dt$ (%/h)
Time (h)

(c)

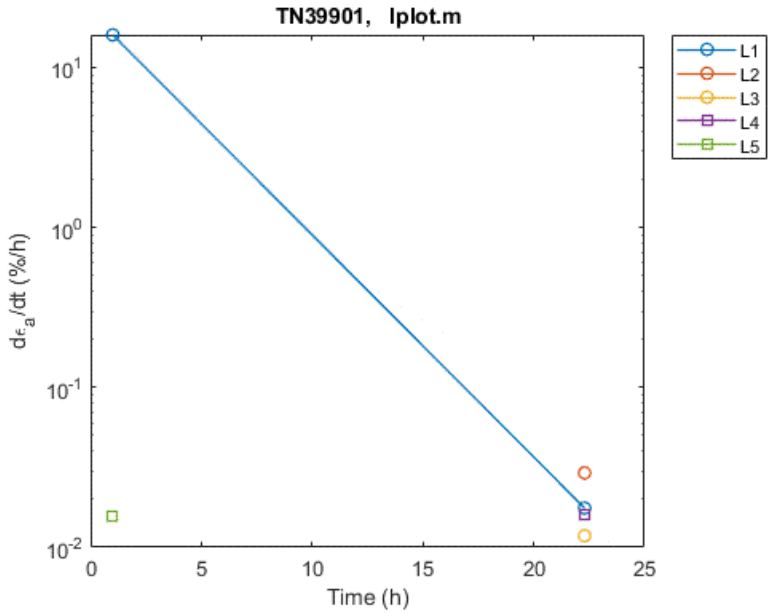

(d)

Figure 9 Variations of (a) axial deformation, (b) axial strain, (c) strain rate, and (d) same as (c) but with log scale in y-axis for GTJ 50/50; 650°C, inner pressure 46.26 MPa (6,710 psi)

Table 3 Axial creep rates of various subsections

Spec.	Subsect.	Equiv. Stress	Stress Gradient	Creep Time	Axial Rate	Ratio of Axial to Tang. Rate
		MPa	MPa/mm	h	%/h	
GTJ 50/50	347H	165		22.3	1.76E-02	1.05
	GTJ	134	5.17	22.3	2.92E-02	1.03
	G91	103		22.3	1.18E-02	0.04
GTJ 100/80/60	347H	165		38	2.40E-04	0.01
	GTJ	134	5.17	38	7.09E-03	0.57
	G91	103		38	3.14E-03	0.02

5.1.2.3 Radial (thickness) strain

The result of radial strain rate is given in Figure 10 with y-axis linear scale in (a), and y axis log scale in (b). Note that there is a negative sign for the y-axis. The negative radial creep rate signifies the wall thinning of tube. A high level of positive radial strain rate was observed at 1 h in GTJ and G91 sections mainly attributed to axial contraction of tube. The positive radial strain rates manifested itself a tendency of wall thickening, remaining to be studied next step. However, the wall thinning of tube prevailed in the final creep stage.

- The largest thinning rate still occurred in the G91 section, ranging from 0.0914 to 0.7257 %/h.
- The magnitude of negative creep rate in the GTJ section was intermediate between 0.0436 and 0.0659 %/h.
- The negative rate in the 347H was much lower than other sections, being from 0.0273 to 0.045 %/h

The results of radial strain rate are summarized in Table 4 for the final creep stage.

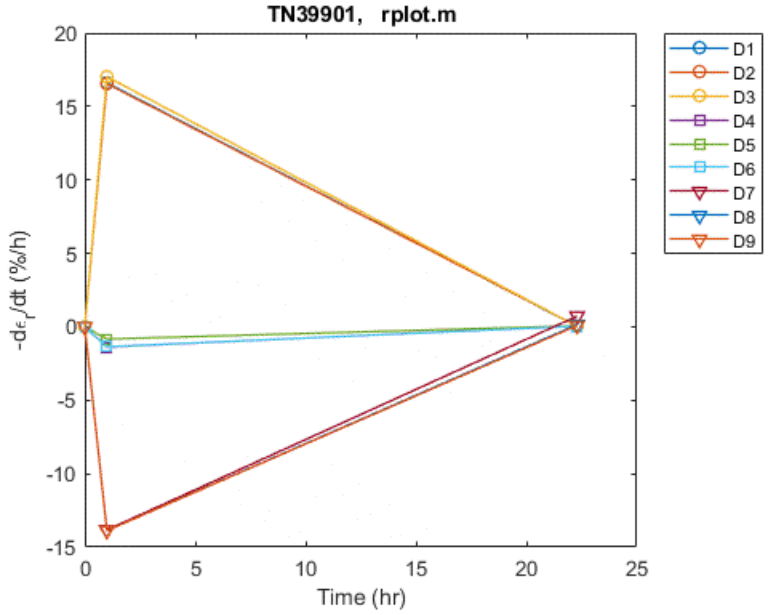

(a)

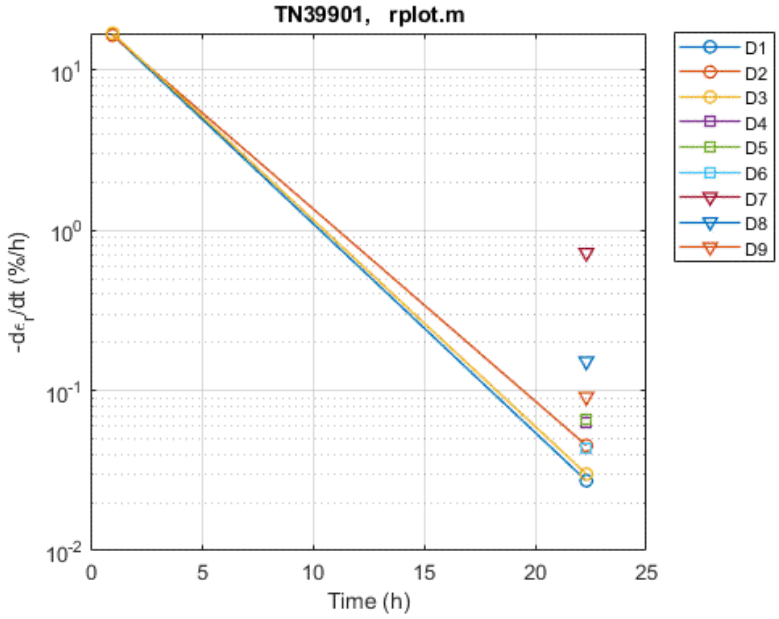

(b)

Figure 10 (a) Variation of negative radial strain rate, and (b) same as (a) with y axis in log scale for GTJ 50/50; 650°C, inner pressure 46.26 MPa (6,710 psi).

Table 4 Radial (thickness) strain rates of various subsections

Spec.	Subsect.	Equiv. Stress	Stress Gradient	Creep Time	Avg. Rad. Rate	Min. Rad. Rate
		MPa	MPa/mm	h	%/h	%/h

GTJ 50/50	347H	165		22.3	-3.43E-02	-4.54E-02
	GTJ	134	5.17	22.3	-5.75E-02	-6.59E-02
	G91	103		22.3	-3.23E-01	-7.26E-01
GTJ 100/80/60	347H	165		38	-2.29E-02	-2.43E-02
	GTJ	134	5.17	38	-1.96E-02	-2.79E-02
	G91	103		38	-1.70E-01	-2.41E-01

5.2 GTJ 100/80/60

5.2.1 Rupture Time

The specimen was tested under a series of temperature and pressure conditions to meet planned project milestone: 1) 650°C, 46.26 MPa (6,710 psi) for 1 h; 2) 600°C, 44.06 MPa (6,680 psi) for 24 h; 3) 400°C, 44.06 MPa for 905h; and 4) 650°C, 46.26 MPa for 37 h (Table 5). The timed data of three thermocouples and pressure transducer are shown in Figure 11, indicating durations of process with various testing conditions.

Failure took place in the G91 subsection in the last test session of 650°C, 46.26 MPa. The creep damage associated with various conditions other than 650°C, 46.26 MPa was estimated only about 1%. Therefore, the creditable creep rupture condition shall be attributed to temperature 650°C, and inner pressure 46.26 MPa with a total time of 38 h.

Again, the rupture time is much lower than the expected. The examination indicated that the creep stress would be 139.27 MPa for a rupture of 38 h. Obviously, this stress level is quite close to the reference stress (140.82 MPa), signifying that failure of the G91 tube followed the reference stress criterion as suggested by the results of specimen GTJ 50/50.

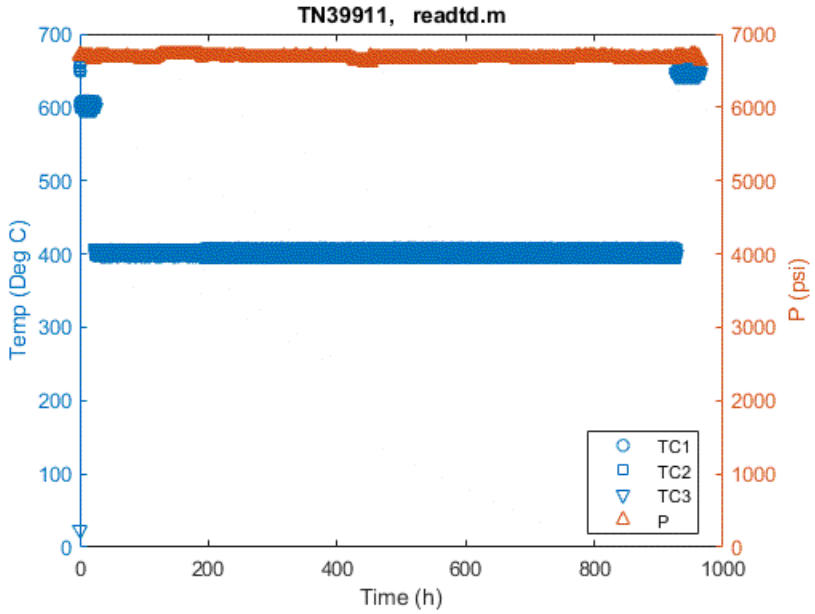

Figure 11 Temperature and pressure profiles for GTJ 100/80/60

Table 5 Summary of test conditions of GTJ 100/80/60

No	Date	Temp (C)	P (psi)	P (MPa)	T_inc (h)	T_acc (h)
1	6/2/2021				0	0
2	7/13/2021	650	6,710	46.26	1	1
3	8/3/2021	600	6,680	44.06	24	25
4	9/11/2021	400	6,680	44.06	167	192
5	10/11/2021	400	6,680	44.06	738	930
6	5/20/2022	650	6,710	46.26	37	967

5.2.2 Creep Deformation

5.2.2.1 Tangential strain

The strain profiles can be found in Figure 12. Compared with that of specimen GTJ 50/50 in Figure 7, general profile pattern is similar; for example, the strain in G91 is much higher than that in GTJ and 347H. The opening in GTJ 100/80/60 again took place in the half of G91 section close to GTJ end; therefore, the largest strain was measured at D7 near opening. The extent of opening in axial direction appears to be larger as validated by the high level of strain at D8. However, the GTJ strain is, in fact, relatively small, forming a local low region in the profile.

The diametric deformation and tangential strain of measurement points are presented in Figure 13. The deformation overall has been mainly developed in the test sessions with 650°C, 46.26 MPa. There was very lower or unmeasurable strain rate during the test sessions under 400°C.

The strain rates of GTJ 100/80/60 are also summarized in Table 2 for the final creep test session. Overall, the strain rate in the GTJ 100/80/60 is lower than in GTJ 50/50, being amounted 44%.

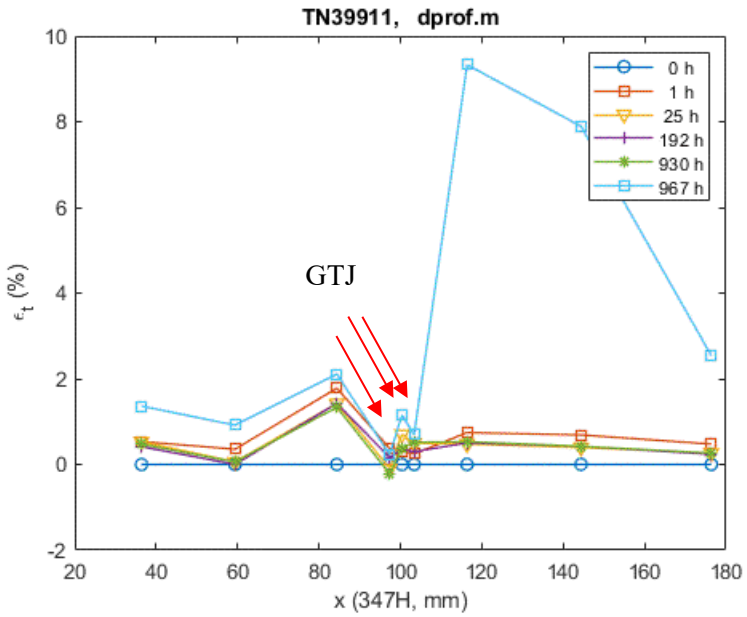

Figure 12 Profiles of tangential strain for GTJ 100/80/60 at various creep times where x is measured from 347H end; 400-650°C, 44.06-46.26 MPa. Three diameter measurement points in GTJ section are indicated by arrows.

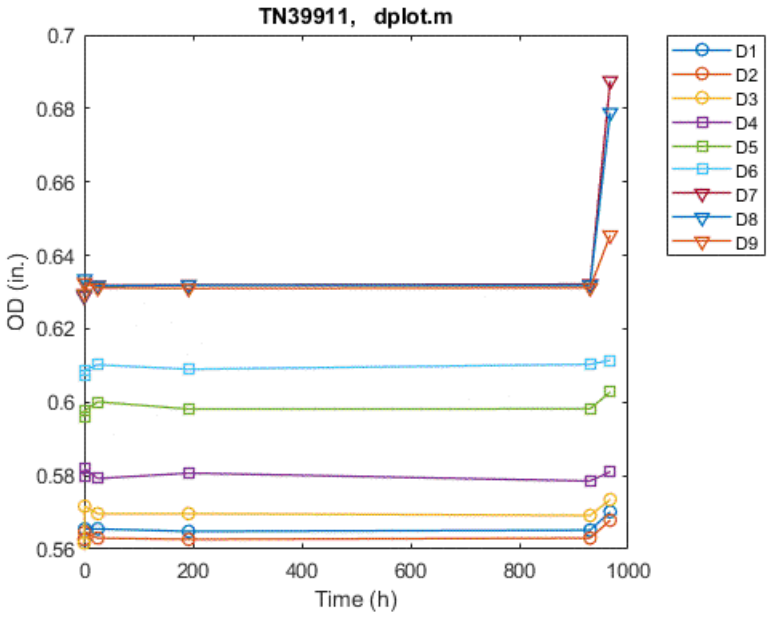

(a)

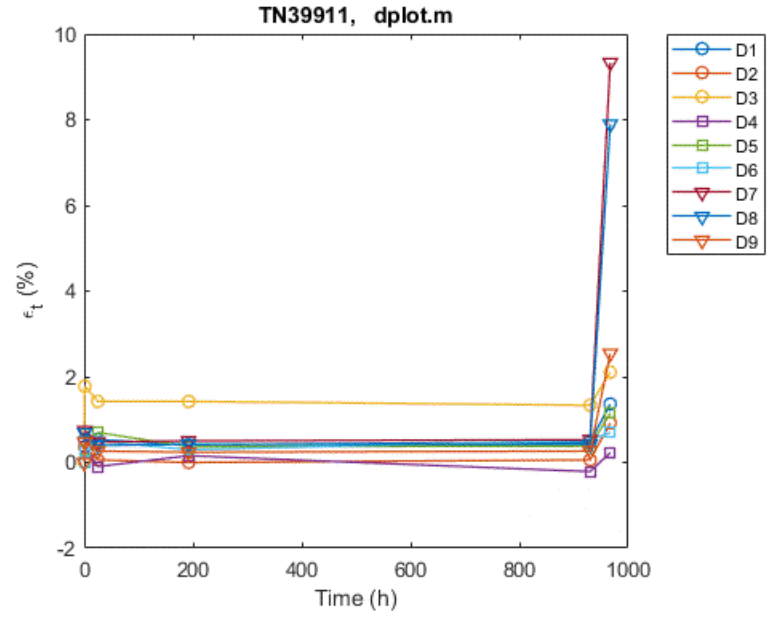

(b)

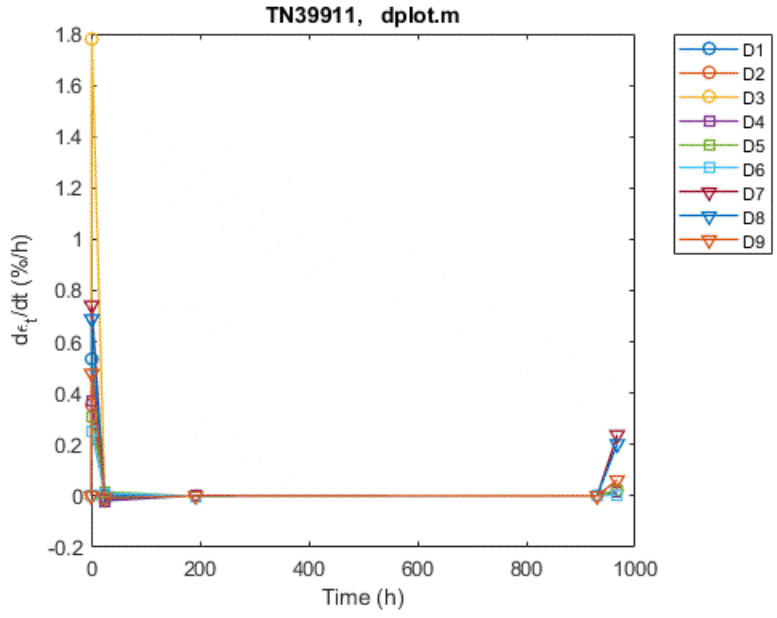

(c)

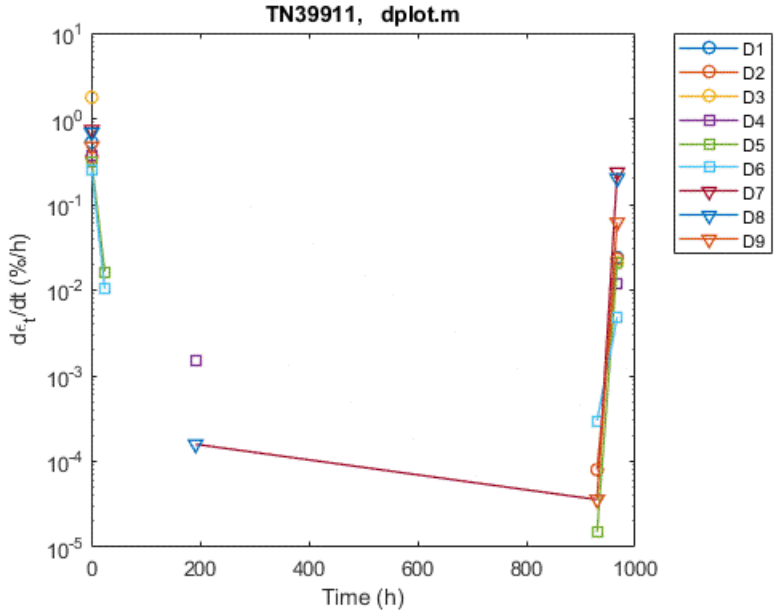

(d)

Figure 13 Variations of (a) diametric deformations, (b) tangential strain; (c) strain rate, (d) same as (c) with log scale in y-axis for GTJ 100/80/60; 400-650°C, 44.06-46.26 MPa

5.2.2.2 Axial strain

There was an appreciable axial strain, above 0.8%, in the GTJ section related to expansion, majority of which was contributed by the loading and first hour creep, as shown in Figure 14. This is different from that with GTJ 50/50 where a contraction of around 2% was seen. Meanwhile, the axial stain of 347H and G91 sections was low at a level of around and less than 0.2%. The contraction was also observed in the G91 section just as that in GTJ 50/50, but the degree of contraction was much lower. The final session of axial strain features a relatively rapid rise in both GTJ and G91 sections.

The axial strain rates of GTJ 100/80/60 for final creep session are also summarized in Table 3. It is clear that the axial stretch rates are generally smaller than those seen in GTJ 50/50.

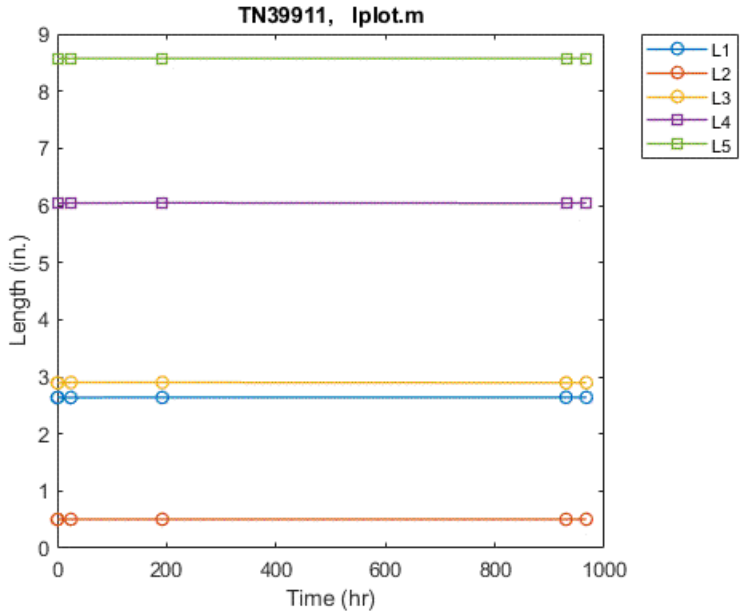

(a)

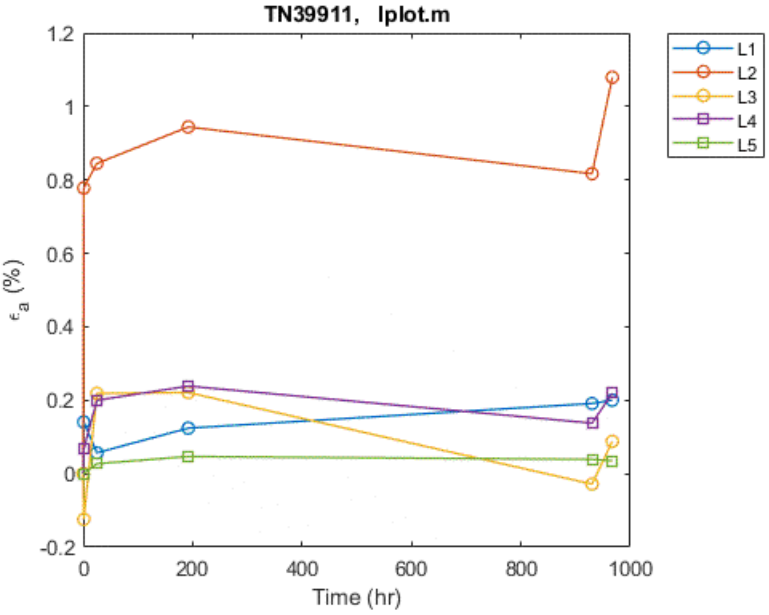

(b)

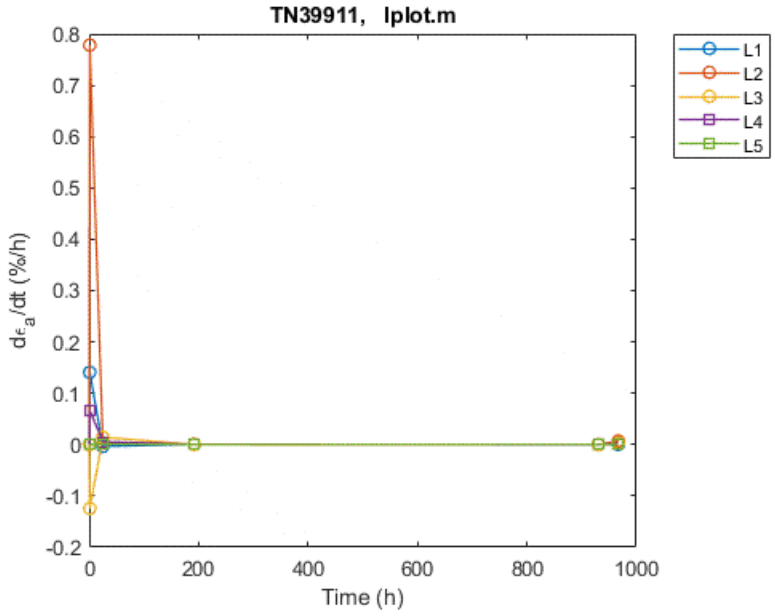

(c)

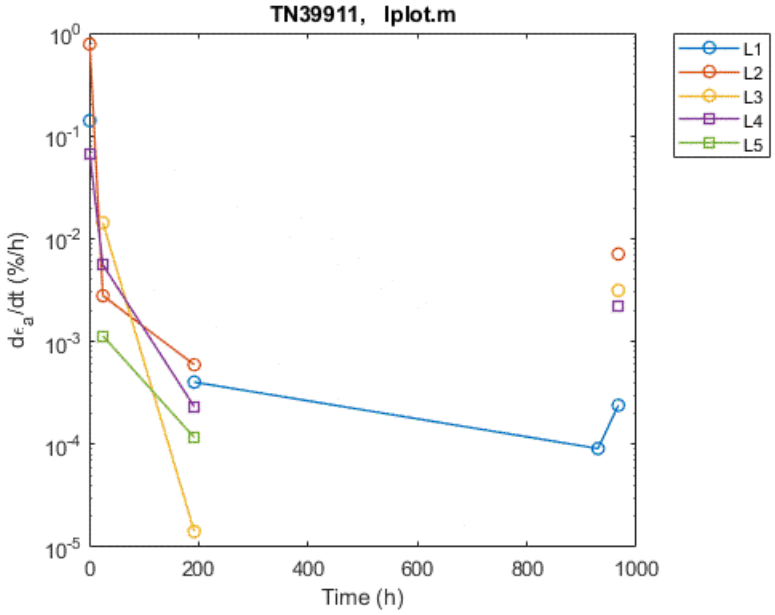

(d)

Figure 14 Variations of (a) longitudinal deformation, (b) axial strain and (c) strain rate, (d) same as (c) with log scale in y-axis for GTJ 100/80/60; 400-650°C, 44.06-46.26 MPa.

5.2.2.3 Radial (thickness) strain

The results for radial strain rate for GTJ 100/80/60 are shown in Figure 15, and the results of final creep session are also summarized in Table 4. In general, the thinning rates of GTJ 100/80/60 are lower than those of GTJ 50/50, including the GTJ section.

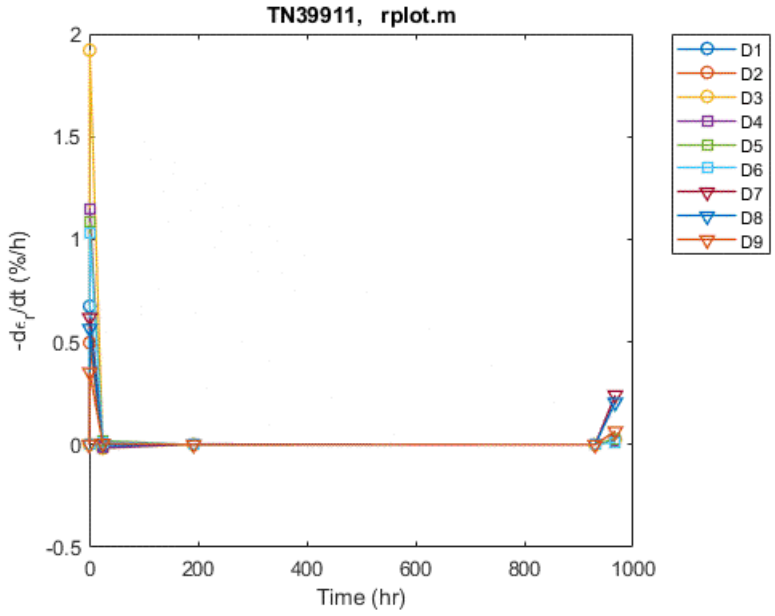

(a)

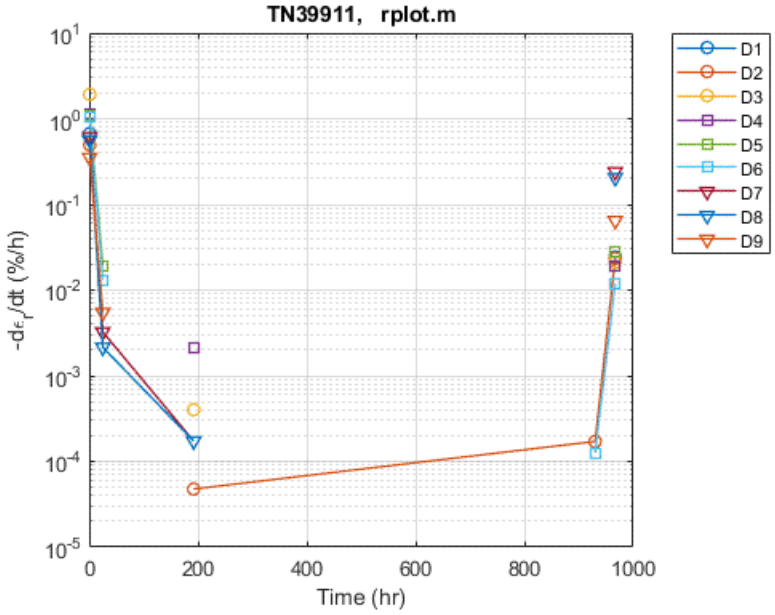

(b)

Figure 15 (a)Variation of radial strain rate and (b) same as (a) with log scale in y-axis for GTJ 100/80/60; 400-650°C, 44.06-46.26 MPa.

5.3 IMAGE OF POST-TEST SPECIMEN

Both the ruptured tube specimens exhibited similar opening location in the G91 subsection. Optical image of the tested specimen is provided in Figure 16 for specimen GTJ 50/50, showing a longitudinal opening developed within the G91 section whose length is about 18 mm, and the cross-

sectional area increased about 37% at the failure position. The G91 section appears very rusty. No microstructural data of the tested specimen are available for the time being.

Figure 16 Image for post-test specimen GTJ 50/50; 650^{o}C, inner pressure 46.26 MPa (6,710 psi), 22.3 h

6. ANALYSIS AND DISCUSSION

6.1 FAILURE CRITERION AND WALL THICKNESS

For the structure involved with multiaxial stresses and multiple materials, the reliability depends on strength and failure criterion of individual components. The analysis was conducted to identify the yield criterion.

The G91 subsection is focused here because it is the position where the creep rupture was observed. As mentioned previously, the ratio of thickness to inner diameter is a little over 0.1 so that the subsection was analyzed as a thick- wall tube. Thus, the averaged value of effective stresses over the thickness was focused. The differences were examined between 1) the observed stresses as manifested by the LM stresses of specimens tested, and 2) the predicted stresses based on various criteria. As a result, the best criterion is identified with one that produces the smallest difference.

The results demonstrated that, although the Mises criterion is widely accepted for ductile structure, the reference stress is more applicable to the G91 tube material than the Mises criterion as can be seen from Table 6.

Table 6 Differences between the predicted stress and observed stress for various criteria

	Mises	**Stress intensity**	**Reference stress**
	MPa	**MPa**	**MPa**
Predicted value	119.79	138.32	140.82
Exp. observation	143.44	143.44	143.44
Difference	23.65	5.12	2.62

By re-writing Equation 6, the wall thickness can be expressed as follows

$$h = R_i[\exp\left(\frac{p}{\sigma_{ref}}\right) - 1].$$

Equation 12

Given stress 103 MPa, pressure 46.26 MPa, and inner radius 5.76 mm, we can have h = 3.26 mm for the G91 section. This is obviously higher than current thickness 2.24 mm in the design. If adapting the new wall thickness, then the OD of G91 section will be 18 mm. A new cycle of specimen design is needed to account for the size and availability of materials.

6.2 CREEP RATE IN G91 SUBSECTION

Let's look at the strain rate obtained in tube creep tests with focus on the G91 subsection. The purpose is to illustrate if the creep rate for a multiaxial loading can be validated from related uniaxial loading data.

For the steady (secondary stage) creep, the creep rate can be assumed to follow Norton's law, namely,

$$\dot{\varepsilon} = B\sigma^n$$

Equation 13

where B and n are Norton parameters, σ is in MPa, and $\dot{\varepsilon}$ is strain rate in %/h. The Norton parameters were n = 8.561, B = 4.29E-20, based on the report by Swindeman and Swindeman.[20]

Two aspects are involved with the application of Norton's law.

1) An equivalent quantity is needed to be substituted for the stress on the right side to account for the multiaxial stress loading according to yield criterion as discussed in Sect. 2.1. Accordingly, an equivalent quantity is needed for the strain rate evaluation on the left side to be described shortly.
2) To accommodate the variation of stress over the wall thickness, an averaged equivalent stress over the wall thickness of tube was used. This consideration somehow agrees with the method used for the deformation measurement of tube. In this study, the change of tube OD was measured, and the calculated tangential strain was taken as the average of that over the wall thickness.

By substituting Norton parameters and the stress condition into the equation, the results were obtained for G91 section as given in Table 7 for the different effective stresses.

The equivalent strain rate can be written for Mises as follows

$$\dot{\varepsilon}_{eq} = \frac{\sqrt{2}}{3}[(\dot{\varepsilon}_1 - \dot{\varepsilon}_2)^2 + (\dot{\varepsilon}_2 - \dot{\varepsilon}_3)^2 + (\dot{\varepsilon}_3 - \dot{\varepsilon}_1)^2]^{1/2}$$

Equation 14

and for stress intensity, there is

$$\dot{\varepsilon}_{eq} = \dot{\varepsilon}_1 - \dot{\varepsilon}_3$$

Equation 15

where the principal strain rates are the tangential, axial, and radial strain rates of tube. The averaged values for the final creep session (Table 2-Table 4) were substituted into the equation resulting in the observed values listed for GTJ 50/50 and GTJ 100/80/60 in Table 7.

By focusing on the D9 (that was less affected by the opening), one can be seen that both criteria predicted a strain rate lower than the observed in the two specimens; the strain rates for the whole G91 section are shown to be generally higher than the predicted because of the accelerated creep and rupture. The reference -based strain rates are a little closer to the predicted than Mises-based strain rate, Table 8.

Table 7 Equivalent strain rate of G91 subsection at temperature 650°C

Criterion	**Avg. σ_{eq}**	**Predicted**	**GTJ 50/50**		**GTJ 100/80/60**	
			D9	**Whole Section**	**D9**	**Whole Section**
	MPa	**%/h**	**%/h**	**%/h**	**%/h**	**%/h**
Mises	119.79	2.66E-02	9.94E-02	3.66E-01	7.29E-02	1.95E-01
Stress intensity	138.32	9.12E-02	1.71E-01	6.34E-01	1.26E-01	3.37E-01
Reference stress	140.82	1.06E-01	1.71E-01	6.34E-01	1.26E-01	3.37E-01

Table 8 Differences between the predicted strain and observed strain at the D9 for various criteria

	Mises	**Stress intensity**	**Reference stress**
	%/h	**%/h**	**%/h**
Predicted value	2.66E-02	9.12E-02	1.06E-01
Exp. observation	8.62E-02	1.49E-01	1.49E-01

Difference	5.96E-02	5.73E-02	4.22E-02

6.3 CREEP RATE IN GTJ SUBSECTION

With the data in Table 2-Table 4, the equivalent strain rates for GTJ subsection were calculated according to Equation 15, and are provided in Table 9.

The equivalent stress of 11.99 mm GJT section was, in fact, varying from 165 MPa in 347H end (Mises-based) to 140.82 MPa in G91 end (reference-based). The end stresses result in an averaged stress of 152.91 MPa over the GTJ subsection with a stress gradient of 2.0 MPa/mm. The resultant averaged stress appears to be higher than what was targeted originally (134 MPa).

The results showed that the strain rate of GTJ subsection is lower in GTJ 100/80/60 than in GTI 50/50, and at the same time, the difference between the averaged and maximum strain rates is small for each specimen. The controlling mechanism remains unclear regarding why GTJ 100/80/60 exhibited a lowered strain rate. Detailed microstructure may be necessary to answer the question.

For a given temperature, the creep rates under various creep stresses are requested if the stress exponent is desired for a better characterization of GTJ materials' creep response.

Table 9 Equivalent strain rate of GTJ subsection

Specimen	**Temp**	**Averaged Equiv. Stress**	**Averaged**	**Maximum**
	Deg C	**MPa**	**%/h**	**%/h**
GTJ 50/50	650	152.91	8.58E-02	1.03E-01
GTJ 100/80/60	650	152.91	3.21E-02	4.86E-02

7. SUMMARY AND FUTURE WORK

7.1 SUMMARY

7.1.1 Experimental Development

A specimen with reduced gage section was designed for the pressurized tube creep testing of printed GTJ. The design targets 500 h rupture time at 650°C. The strength would be 165 MPa for 347H and 103 MPa for G91. A specimen with tapered GTJ section has been introduced to accommodate the different creep strengths for a uniform lifetime throughout the GTJ specimen.

- 347H section: OD 14.33 mm, wall thickness 1.40 mm, ID 11.52 mm, length 71.58 mm.
- G91 section: OD 16.0 mm, wall thickness 2.24 mm, ID 11.52 mm, length 80.01 mm.
- GTJ section: OD 14.33 - 16.0 mm, ID 11.52 mm, length 11.99 mm.

Two specimens, GTJ 50/50 and GTJ 100/80/60, were prepared by using GTAW.

A pressure of 46.26 MPa (6,710 psi) has been proposed to achieve the desired rupture time. A tube testing stage was identified for this task. The instruments and facilities for controls and measurements were calibrated and inspected for the proposed tests.

The deformation of specimen was monitored and measured offline at room temperature. At periodical interruptions, the system was depressurized and cooled, and specimen taken out for inspection and measurement.

7.1.2 Experimental Observation

The pressurized tube creep tests of GTJ 50/50 and GTJ 100/80/60 were completed at temperature 650°C, inner pressure 46.26 MPa. Both specimens failed in the G91 section near the GTJ section with a sizable longitudinal opening. Both GTJs survived the creep loading.

The rupture times (22.3 - 38 h) were much shorter than the expected. The discrepancy highlights the following aspects: 1) failure of dissimilar base metals may follow different criteria; 2) for the G91, reference stress can be more effective in predicting the rupture life than Mises criterion.

The creep rate in the GTJ section of GTJ 100/80/60 has been shown to be lower than in GTJ 50/50. The underline mechanism for the lowered creep rate in the former remains to be explored. Meanwhile, the creep rate in base metals like the G91 was demonstrated to follow Norton's law.

7.2 NEXT STEP

It is expected that at least following respects can be pursued in the future:

- Perform uniaxial creep test for GTJ
- Perform additional tests under conditions for at least several thousands of hours of creep or rupture time if printed GTJ materials are available.
- Perform microstructural analysis on the tested specimens to investigate controlling creep/ failure mechanisms.
- Conduct numerical study to understand the deformation and failure mechanisms.

ACKNOWLEDGEMENTS

The work was funded by US DOE FE program under DOE contract DE-AC05-00OR22725 with UT-Battelle, LLC.

Authors appreciate many individuals of ORNL for their helpful discussion and great support. Particularly, we would like to thank Seth Baird for preparing engineering drawing, Doug Kyle for welding, Doug Stringfield for the coordination of specimen machining, Dean Freeman for the dimension inspection of specimens, Drew Walker for the instrument calibration, Shane Hawkins, Michael Roberts, Eric Vidal for the coordination and inspection of pressure system. Authors also want to thank Drs. Lianshan Lin and Jian Chen of ORNL for their review and constructive comments.

REFERENCES

[1] V. K. Sikka, G. M. Goodwin, J. F. King, and K. V. Cook, 1984, Fabrication of Modified 9Cr-1Mo Steel Test Article for Exposure in Sodium Components Test Loop at Energy Technology Engineering Center, ORNL-6034, Oak Ridge National Laboratory, April 1984.

[2] R. Mittal, B. S. Sidhu, 2015, Microstructures and mechanical properties of dissimilar T91/347Hsteel weldments, J. Mater. Proc. Tech., 220, 76-86.

[3] N. Kumar E., G. D. J. Ram, K. Devakumaran, R. S. Kottada, 2020, Effect of long-term exposure at 650 °C on microstructural and creep characteristics of T92/Super304H dissimilar welds, Welding in the World, 64, 467-481.

[4] A. Kulkarni, D. K. Dwivedi, M. Vasudevan, 2020, Microstructure and mechanical properties of A-TIG welded AISI 316L SS-Alloy 800 dissimilar metal joint, Mater. Sci. & Eng. A 790, 139685.

[5] J.D. Parker, G.C. Stratford, 2001, The high-temperature performance of nickel-based transition joints I. Deformation behaviour, Mater. Sci. and Eng. A299, 164–173.

[6] S. Huysmans, J. Vekeman, C. Hautfenne, 2017, Dissimilar metal welds between 9Cr creep strength enhanced ferritic steel and advanced stainless steels—creep rupture test results and microstructural investigations, Weld World, 61, 341-350.

[7] Y. Zhang, K. Li, Z. Cai, J. Pan, 2019, Creep rupture properties of dissimilar metal weld between Inconel 617B and modified 9%Cr martensitic steel, Mater. Sci. & Eng., A 764, 138185.

[8] M. Sireesha, S. K. Albert, and S. Sundaresan, 2005, Influence of High-Temperature Exposure on the Microstructure and Mechanical Properties of Dissimilar Metal Welds between Modified 9Cr-1Mo Steel and Alloy 800, Metallurgical and Materials Transactions A, 36A 1495-1506.

[9] T. Totemeier, 2018, Dissimilar metal welds in Grade 91 steel, News and Views, Structural Integrity Associates, Inc., 44, 15-18.

[10] G. J. Brentrup, B. S. Snowden, J. N. Dupont, and J. L. Grenestedt, 2012, Design considerations of graded transition joints for welding dissimilar alloys, Welding Journal, 91, 252-s-259-s.

[11] J. N. DuPont, 2012, Microstructural evolution and high temperature failure of ferritic to austenitic dissimilar welds, International Materials Reviews, 57:4, 208-234.

[12] P. Mayr, C. Schlacher, J. A. Siefert & J. D. Parker, 2019, Microstructural features, mechanical properties and high temperature failures of ferritic to ferritic dissimilar welds, International Materials Reviews, 64:1, 1-26.

[13] I. Finnie and W. R. Heller, 1959, Creep of Engineering Materials, McGraw-Hill, pp.182-184.

[14] R. W. Swindeman, M. J. Swindeman, B. W. Roberts, B. E. Thurgood, D. L. Marriott, 2007, Verification of Allowable Stresses in ASME Section III, Subsection NH for Grade 91 Steel, Part 1: Base Metal, Sept. 2007.

[15] AISI, High-Temperature Characteristics of Stainless Steels, NiDI.

[16] F. A. Garner, C. R. Eiholzer, M. L. Hamilton, D. R Duncan, R. J. Puigh, M.B. Toloczko, A. S Kumar, 1993, The influence of specimen size on measurement of thermal or irradiation creep in pressurized tubes, Effects of Radiation on Materials: 16th International Symposium, ASTM STP 1175, A. S. Kumar, D. S. Gelles and R. K. Nanstad, Eds., American Society for Testing and Materials, Philadelphia, 1993.

[17] H. Tsai, and M. C. Billone, 2006, Thermal creep of irradiated Zircaloy cladding, Journal of ASTM International, 3, Paper ID JAI12425.

[18] W. Li, R. A. Holt, 2010, Anisotropic thermal creep of internally pressurized Zr–2.5Nb tubes, Journal of Nuclear Materials, 401 25–37.

[19] H.-M. Tung, K. Mob, J. F. Stubbins, 2014, Biaxial thermal creep of Inconel 617 and Haynes 230 at 850 and 950°C, Journal of Nuclear Materials, 447, 28–37.

[20] R. W. Swindeman and M. J. Swindeman, 2015, A Compilation of Creep Curves for 9Cr-1Mo-V Steel and the Recommendation of a Creep Law for the Construction of Isochronous Stress-Strain Curves, Cromtech Inc, Mar 31, 2015.